A Circuit Model Accounting for the Frequency-Dependent Behavior of Electrical Machine Windings

Kaoutar Hazim[1,2], Guillaume Parent[1], Stéphane Duchesne[1] and Christophe Geuzaine[2]
[1]Univ. Artois, UR 4025, Laboratoire Systèmes Électrotechniques et Environnement (LSEE), Béthune, F-62400, France
[2]Department of Electrical Engineering and Computer Science, Montefiore Institute, University of Liege, Liège B-4000, Belgium

This paper presents a method to take into account, in a circuit model, the frequency-dependent behavior of electrical machine windings. First, the frequency-dependent inductances (both self and mutual) and resistances are determined thanks to time harmonic finite element (FE) computations in the frequency range of interest. The frequency-dependent behavior of the capacitances is investigated and the choice of using an electrostatic model is justified. Then, the different frequency-dependent parameters are included in a circuit model using behavioral voltage sources placed in series, which allows to forego using delicate fitting techniques within large scale lumped parameter models. Time-domain node voltages are then computed by reducing the circuit to the nodes of interest through the extraction of a reduced, frequency-dependent, nodal admittance matrix. An inverse fast Fourier transform can be readily applied to obtain the time evolution of inter-turn winding voltages. Alternatively, using vector fitting on the reduced equivalent circuit can further improve results by ensuring passivity and filtering unphysical high-frequency modes, with reasonable computational overhead. This enables the usage of the proposed method as a diagnostic tool before or during the phase of electrical winding design. A test winding with 69 turns is used for validation. An excellent agreement between experimental and simulation results is observed both in the frequency- and in the time-domain.

***Index Terms*—Finite element method, frequency-dependent parameters, finite element simulation, time-domain simulation, frequency-domain simulation, vector fitting, inverse fast Fourrier transform.**

I. Introduction

THE new generation of semiconductor devices imposes high steep-fronted voltages, which ends up generating intense inter-turn electric fields in the winding of electrical machines. When these high electric fields exceed the partial discharge inception voltage, partial discharges occur. The latter may result in an inter-turn local fault, which increases the thermal stress that electrical machines have to withstand. Accordingly, an expansion of the local fault followed by an eventual premature breakdown of the machines can take place. Thus, the need of a well parameterized model of the machines windings that will serve as a predictive diagnostic tool. An easy to implement but quite efficient method to evaluate the occurrence probability of partial discharge between two electrodes is to compare the electric field strength located between those electrodes to the Paschen's law [1]. It has been shown in [2,3] that this can be entirely done by means of finite element (FE) computations if one knows the voltage between the considered electrodes. Hence, applying this method to the case of a machine winding requires the computation of inter-turn voltages, which can be achieved by means of a Lumped Parameter Model (LPM) [4]–[6].

Mihaila *et al* [4] introduced a phenomenological LPM based on an elementary cell that models a single turn and that allows to account for self resistive as well as both self and mutual inductive and capacitive phenomena. Then, the LPM allowing to deal with a whole winding is obtained by simply repeating this elementary cell as many times as the number of its composing turns. The main limitation of the approach presented in [4] lies in the evaluation of the circuit parameters: while some are evaluated numerically, at a single frequency, rough analytical approximations or experimental measurements are used for others, making the resulting LPM ill-suited for uses as a predictive tool for inter-turn winding voltages. Toudji *et al* [5] partially overcame those drawbacks by computing all the lumped parameter values by means of FE computations. However, all the parameters are computed at the first resonance frequency only, and inter-turn coupling losses linked to proximity effects are not taken into account.

This paper presents an improved methodology to include the different couplings between turns and to take into account the frequency dependency of the LPM elements. In the frequency domain, the different frequency-dependent parameters are included in a circuit model using behavioral voltage sources. This allows to forego using delicate fitting techniques within large scale lumped parameter models, which are notoriously difficult to make robust [7]. Time-domain node voltages are then computed by reducing the circuit to the nodes of interest through the extraction of a reduced, frequency-dependent nodal admittance matrix, followed by an Inverse Fast Fourier Transform (IFFT). Alternatively, vector fitting can be applied on the *reduced* equivalent circuit, which can further improve inter-turn winding voltages by ensuring passivity and by filtering unphysical high-frequency modes, at the cost of a (very fast) time-domain circuit simulation per node of interest. This enables the usage of the proposed method as a diagnostic tool before or during the phase of electrical winding design.

This paper is organized as follows. First, the topology of the elementary cell composing the LPM is presented in Section II, together with the FE identification procedure for each parameter, including their frequency behavior. Section III then presents the new circuit model in the frequency domain, before detailing its reduction to the nodes of interest for time domain simulations. In Section IV, the methodology is validated against experimental measurements performed on a 69-turns winding, and its added value compared to the

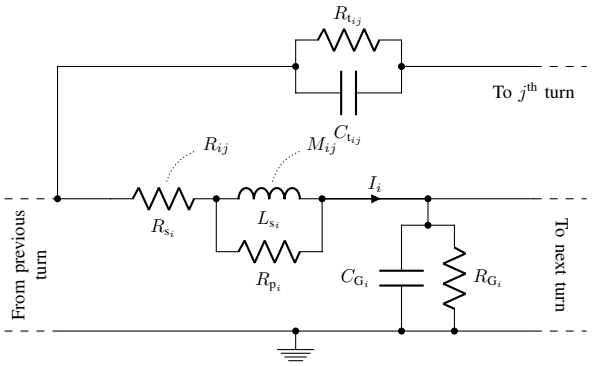

Fig. 1. Elementary cell of turn i of a winding.

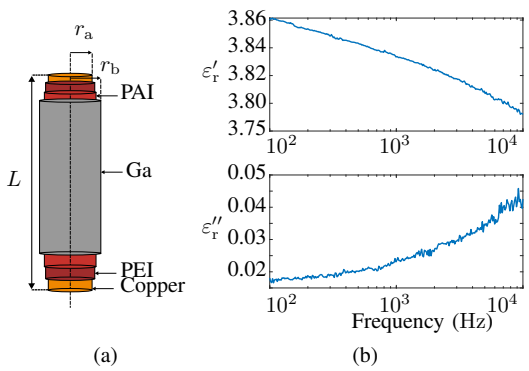

Fig. 2. (a) Capacitive measurement setup. (b) Variation of the real and imaginary parts of the permittivity.

previous approach is highlighted.

II. Lumped parameter identification accounting for frequency dependence

A. Elementary cell

Fig. 1 shows the elementary cell of one turn of the winding considered in this work. It allows to represent each of the occurring physical phenomena (resistive, inductive and capacitive) within a winding. Iron losses, Joule losses and dielectric losses (turn-to-turn and turn-to-ground) are modeled using resistances R_{p_i}, R_{s_i}, $R_{\mathrm{t}_{ij}}$, and R_{G_i}, respectively. The appearing electromotive force across each turn i is modeled using an inductance L_{s_i}. The resistive and inductive coupling phenomena with turn j are modeled by means of mutual resistances [8] and inductances R_{ij} and M_{ij} respectively. Finally, the capacitive couplings (turn-to-turn and turn-to-ground) are modeled using the capacitances $C_{\mathrm{t}_{ij}}$ and C_{G_i}, respectively.

Compared to the elementary cell proposed in [5], the resistance R_{ij} is new, and all parameters can be considered as frequency-dependent if need be.

B. Inductive phenomena and Joule losses

Let us define the self and mutual impedances $\overline{Z}_{\mathrm{s}_i}$ and $\overline{Z}_{\mathrm{m}_{ij}}$:

$$\overline{Z}_{\mathrm{s}_i} = \frac{\overline{U}_i}{\overline{I}_i} = R_{\mathrm{s}_i} + j\, L_{\mathrm{s}_i}\, \omega \tag{1}$$

$$\overline{Z}_{\mathrm{m}_{ij}} = \frac{\overline{U}_j}{\overline{I}_i} = R_{ij} + j\, M_{ij}\, \omega \tag{2}$$

where as above i and j refer to the considered turn and any other turn of the winding respectively. Then, the self – R_{s_i} and L_{s_i} – and the mutual – R_{ij} and M_{ij} – parameters can easily be deduced from (1) and (2) by setting the current in the i^{th} turn to a given value I_i while remaining the current in all the other turns to 0 A. The two resistances R_{s_i} and R_{ij} model Joule losses, including skin and proximity effects respectively, while L_{s_i} and M_{ij} account for the self and mutual inductive effects. Turn voltages U_i and U_j are obtained through the solution of as many frequency-domain magnetodynamic problems as there are turns times the number of frequencies of interest. A standard 2D-axisymmetric magnetodynamic FE formulation in terms of the magnetic vector potential is used in our numerical investigations, implemented in the open source GetDP software [9].

C. Core losses

The resistance R_{p_i} models core losses. It can be computed using *a posteriori* Steinmetz-like formulas, or be extracted directly from the magnetodynamic FE resolutions if it includes core loss model. In the experimental validations presented in Section IV the winding has no core and R_{p_i} is thus simply disregarded.

D. Capacitive phenomena and dielectric losses

Investigating the frequency behavior of the capacitive coupling amounts to studying the response to the frequency increase of the complex permittivity $\overline{\varepsilon}_{\mathrm{r}}(f) = \varepsilon'_{\mathrm{r}}(f) - j\varepsilon''_{\mathrm{r}}(f)$ of the used dielectric materials. The real part represents the stored electric energy, modeled by C_{t_i} and C_{G_i}, whereas the imaginary part represents the dielectric losses, modeled with R_{t_i} and R_{G_i} in Fig. 1. The wires classically used in machine windings are two layered: Polyester-imide (PEI) as the first layer with Polyamide-imide (PAI) on top. We used a wire sample and further coated it with Gallium (Ga) as illustrated in Fig. 2a, in order to create a capacitance and measure the impedance

$$\overline{Z}_{\mathrm{c}}(f) = \frac{1}{j\overline{C}(f)\omega} = \frac{\ln\left(\frac{r_{\mathrm{b}}}{r_{\mathrm{a}}}\right)}{2j\pi L\varepsilon_0\overline{\varepsilon}_{\mathrm{r}}(f)\omega} = \left(\frac{1}{R} + jC\omega\right)^{-1}, \tag{3}$$

with r_{a}, r_{b}, L, ε_0, ω and $\overline{C}$ being the internal and external radii, the length of the sample, the vacuum permittivity, the angular frequency and the complex capacitance of the dielectric. The variations of $\varepsilon'_{\mathrm{r}}(f)$ and $\varepsilon''_{\mathrm{r}}(f)$ up to 10 kHz are presented in Fig. 2b. As there is only a 5 % variation in $\varepsilon'_{\mathrm{r}}(f)$ over two decades it can safely be assumed as constant w.r.t. frequency. Unlike in previous work [5] however, where R_{t} was assigned a constant value extracted from experimental measurements, here we compute its value numerically using a frequency-domain electrostatic-type FE formulation in terms of the electric scalar potential. In way similar to what was carried out in Section II-B, each conductor is set to a chosen voltage value V_i while the others are set to 0 V, leading to as many calculations as there are turns. The capacitances $C_{t_{ij}}$ and resistances $R_{t_{ij}}$ are then deduced from the computed (complex-valued) charges, again using GetDP. The coupling to the ground (C_{G_i} and R_{G_i}) is accounted for through the remaining spacial charges.

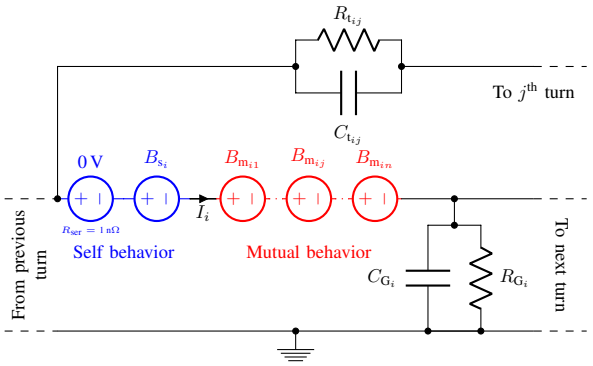

Fig. 3. Proposed frequency-dependent elementary cell.

III. The Proposed Circuit Model

A. Frequency-domain

After computing the different parameters in the frequency range of interest (typically extending from $f_1 = 40\,\text{Hz}$ up to $f_\text{m} = 110\,\text{MHz}$), the values can be gathered in matrices that are stored in LTspice tables.

The proposed frequency-domain elementary cell is depicted in Fig. 3, where B_{s_i} contains the frequency-dependent values of $\overline{Z}_{s_i}(f) = R_{s_i}(f) + jL_{s_i}(f)\omega$ modeling the self behavior of the i^{th} turn, whereas $B_{m_{i1}}$, $B_{m_{ij}}$ and $B_{m_{in}}$ contain the frequency-dependent values of the coupling between turn i and turn 1, between turn i and turn j and between turn i and turn n respectively, and links them to their respective currents. The corresponding expressions are: $\overline{Z}_{i1}(f) = R_{i1}(f) + jM_{i1}(f)\omega$, $\overline{Z}_{ij}(f) = R_{ij}(f) + jM_{ij}(f)\omega$ and $\overline{Z}_{in}(f) = R_{in}(f) + jM_{in}(f)\omega$. The 0 V voltage source, used as a current sensor, contains a 1 nΩ series internal resistance R_ser to avoid having parallel voltage sources. Hence, not only the frequency-dependency of the self behavior is accounted for, but that of the coupling between turns as well. Note that using such behavioral voltage sources allows to forego using delicate fitting techniques within the large scale equivalent circuit, which are notoriously difficult to make robust [7].

B. Time-domain

Given the nature of the proposed frequency-domain elementary cell, its usage in transient simulations is not possible. To account for the different frequency variations in the time-domain, we make use of the reduced nodal admittance matrix

$$\overline{\mathbf{Y}}_n^\text{m} = \begin{pmatrix} \ddots & & \\ & \begin{pmatrix} \overline{Y}_{11}(f_\text{m}) & \overline{Y}_{12}(f_\text{m}) \\ \overline{Y}_{21}(f_\text{m}) & \overline{Y}_{22}(f_\text{m}) \end{pmatrix} & \\ & & \ddots \end{pmatrix}$$
$$\begin{pmatrix} \overline{Y}_{11}(f_1) & \overline{Y}_{12}(f_1) \\ \overline{Y}_{21}(f_1) & \overline{Y}_{22}(f_1) \end{pmatrix} \ddots$$

This matrix is deduced from the frequency circuit model by inspection by first exciting the input node of the winding (*i.e.* the first turn) while short circuiting the node of interest to extract the values $\overline{Y}_{11}(f)$ and $\overline{Y}_{12}(f)$. Then, the first node is short circuited while the node of interest is excited to extract the values $\overline{Y}_{21}(f)$ and $\overline{Y}_{22}(f)$ of the matrix. The circuit is thus reduced to the input node of the winding and the node of interest labeled k, as seen in Fig. 4 where $\overline{V}_1(f)$ and $\overline{V}_\text{k}(f)$ are the spectrum of the imposed voltage on the winding and the

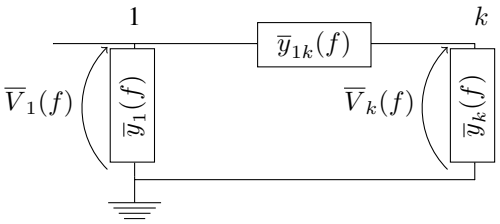

Fig. 4. Equivalent circuit reduced to the k^{th} node.

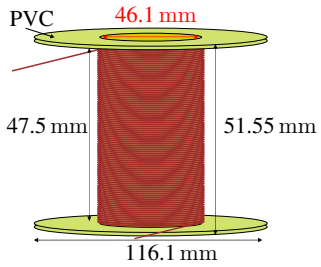

Fig. 5. The 3D geometrical definition of the 69 turns winding.

voltage spectrum of the k^{th} node, respectively. The admittances $\overline{y}_1(f)$, $\overline{y}_\text{k}(f)$ and $\overline{y}_{1\text{k}}(f)$ are computed as follows [10]:

$$\begin{cases} \overline{y}_1(f) = \overline{Y}_{11}(f) + \overline{Y}_{12}(f), \\ \overline{y}_k(f) = \overline{Y}_{22}(f) + \overline{Y}_{21}(f), \\ \overline{y}_{1k}(f) = -\overline{Y}_{12}(f) = -\overline{Y}_{21}(f). \end{cases} \tag{4}$$

Deducing the k^{th} voltage spectrum is straightforward:

$$\overline{V}_k(f) = \overline{V}_1(f) \cdot \frac{\overline{y}_k(f)^{-1}}{\overline{y}_k(f)^{-1} + \overline{y}_{1k}(f)^{-1}}, \tag{5}$$

to which an IFFT is applied.

Alternatively, since the reduced equivalent circuit is (very) small, vector fitting can be applied without the stability concerns encountered when incorporating it in large scale circuits. After applying passivity constraints, the resulting time-domain equivalent circuit can then be simulated by a circuit simulator such as LTspice without issues, with the added benefit that it naturally filters unphysical high-frequency modes compared to the IFFT.

IV. Experimental Validation

In order to validate the methodology experimentally, we consider a two-layered $n = 69$ turns coil wound on PVC with no magnetic core. Its geometrical definition is given in Fig. 5, with 35 turns in the first layer and 34 turns in the second layer. The conductors have a copper diameter $d_\text{c} = 1.25\,\text{mm}$, an insulation thickness of $\ell_\text{insul} = 49.5\,\mu\text{m}$ and a turn-to-turn spacing of $e_\text{it} = 7.91\,\text{mm}$. Although the wire has two dielectric layers (PEI and PAI), we only considered the presence of PEI, given the little information on their respective thicknesses. The PEI and PVC have a relative permittivity of $\varepsilon_{\text{r}_\text{PEI}} = 3.5 - j0.5$ and $\varepsilon_{\text{r}_\text{PVC}} = 4$, respectively.

A. Frequency-domain validation

The impedance measurement is performed using the impedance analyser Agilent 4980A. Fig. 6 compares the experimental results with the proposed model, as well as with the

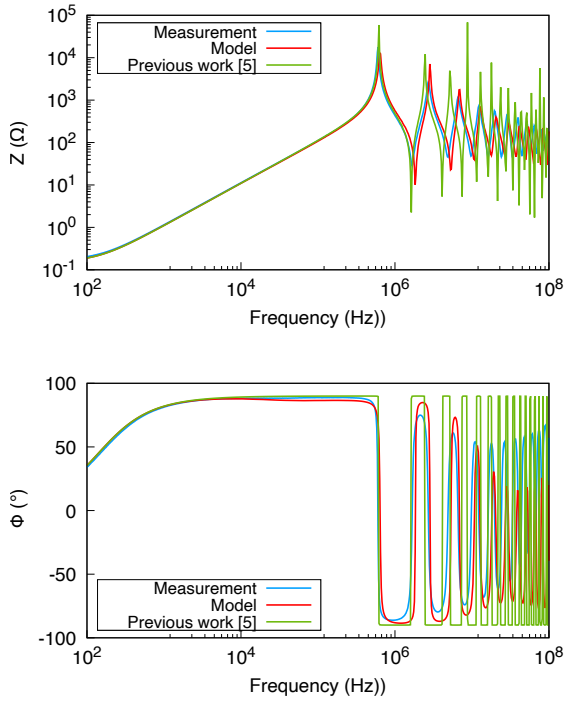

Fig. 6. Frequency response of the 69-turn test winding.

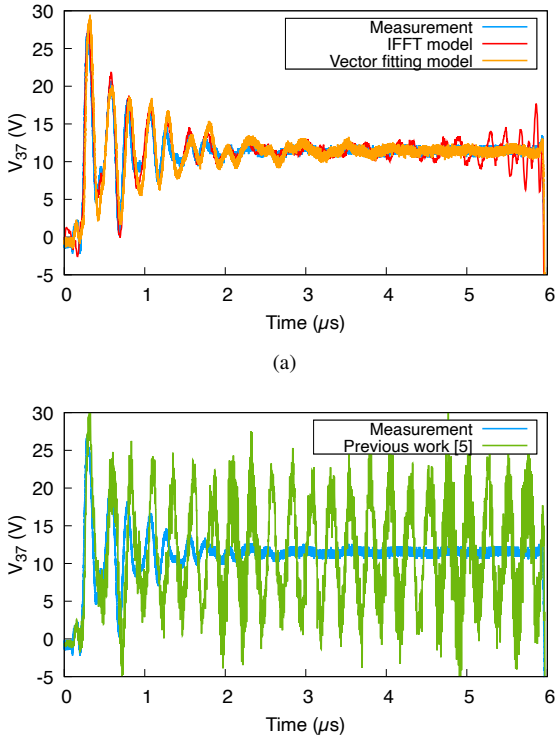

Fig. 7. Evolution of the 37th nodal voltage using (a) IFFT and vector fitting models and (b) model from previous work [5].

previous model from [5], from 40 Hz to 110 MHz. An excellent agreement is shown between experiments and the proposed model on the full frequency range, whereas the previous model only correctly captures the lower frequency band. This clearly demonstrates the added benefit of the proposed approach.

B. Time-domain validation

The experimental setup used for time-domain validation links a converter that switches at 10 kHz with a duty cycle of 2 % to the considered winding through a cable. The supplied input DC voltage was fixed to $V_{\mathrm{DC}} = 25$ V. Fig. 7a shows the time evolution of the voltage on the 37th turn of the winding. When applying the IFFT directly the initial transient is very well captured, but spurious oscillations can be noted at the end of the period. Theses spurious oscillations are strongly reduced by applying vector fitting on the small reduced frequency-dependent admittance matrix, leading to an excellent agreement with experimental results. As a comparison, applying the previous model from [5] is clearly not satisfactory, as illustrated in Fig. 7b.

V. Conclusion

In this paper we have presented a methodology to account for the frequency-dependent behavior of the lumped parameter models of electrical machine windings, in view of predicting inter-turn voltages both in the frequency- and time-domain. The proposed method significantly improves on previous attempts [4,5] and is fully automatic.

Acknowledgment

This work is co-financed by the European Union with the financial support of European Regional Development Fund (ERDF), French State and the French Region of Hauts-de-France, as well as the University of Liege.

References

[1] G. Galli, H. Hamrita, C. Jammes, M. J. Kirkpatrick, E. Odic, P. Dessante, and P. Molinié, "Paschen's law in extreme pressure and temperature conditions," *IEEE Transactions on Plasma Science*, vol. 47, no. 3, pp. 1641–1647, 2019.

[2] G. Parent, M. Rossi, S. Duchesne, and P. Dular, "Determination of Partial Discharge Inception Voltage and Location of Partial Discharges by Means of Paschen's Theory and FEM," *IEEE Transactions on Magnetics*, vol. 55, no. 6, pp. 1–4, Jun. 2019.

[3] T. Mathurin, S. Duchesne, and G. Parent, "Assessment of Finite Element Simulation Methodologies for the Use of Paschen's Law in the Prediction of Partial Discharge Risk in Electrical Windings," *IEEE Access*, vol. 8, pp. 144 557–144 564, Jul. 2020.

[4] V. Mihaila, S. Duchesne, and D. Roger, "A simulation method to predict the turn-to-turn voltage spikes in a PWM fed motor winding," *IEEE Transactions on Dielectrics and Electrical Insulation*, vol. 18, no. 5, pp. 1609–1615, Oct. 2011.

[5] M. Toudji, G. Parent, S. Duchesne, and P. Dular, "Determination of Winding Lumped Parameter Equivalent Circuit by Means of Finite Element Method," *IEEE Transactions on Magnetics*, vol. 53, no. 6, pp. 1–4, Jun. 2017.

[6] S. Bauer, W. Renhart, and O. Biro, "FEM-based computation of circuit parameters for testing fast transients for EMC problems," *IEEE Transactions on Magnetics*, vol. 53, no. 6, pp. 1–4, Jun. 2017.

[7] B. Gustavsen, "Computer code for rational approximation of frequency dependent admittance matrices," *IEEE Transactions on Power Delivery*, vol. 17, no. 4, pp. 1093–1098, Oct. 2002.

[8] J. Spreen, "Electrical terminal representation of conductor loss in transformers," *IEEE Transactions on Power Electronics*, vol. 5, no. 4, pp. 424–429, Oct. 1990.

[9] C. Geuzaine, "GetDP: a general finite-element solver for the de Rham complex," in *PAMM: Proceedings in Applied Mathematics and Mechanics*, vol. 7, no. 1. Wiley, 2007, pp. 1 010 603–1 010 604.

[10] N. Deo, *Graph theory with applications to engineering & computer science*, D. Publications, Ed. New York, NY: Mineola, 1974.